Sensors & Actuators: B. Chemical 427 (2025) 137134

Contents lists available at ScienceDirect

Sensors and Actuators: B. Chemical

journal homepage: www.elsevier.com/locate/snb

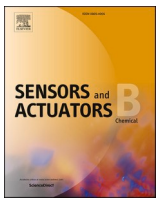

Ultrasensitive miRNA-135a-5p biochip for early Alzheimer's disease detection utilizing magneto-optical faraday effect and magnetoplasmonic nanoparticles

Chin-Wei Lin [a], Jing-Han Huang [b], Po-Han Lin [c], Ting-Bin Chen [d], Li-Min Wang [a], Yu-Ching Huang [e,f,*], Kuen-Lin Chen [b,g,*]

[a] Department of Physics, National Taiwan University, Taipei 106, Taiwan
[b] Institute of Nanoscience, National Chung Hsing University, Taichung 402, Taiwan
[c] Department of Medical Genetics, National Taiwan University Hospital, Taipei 100225, Taiwan
[d] Department of Neurology, Neurological Institute, Taichung Veterans General Hospital, Taichung 407, Taiwan
[e] Department of Materials Engineering & Biochemical Technology R&D Center, Ming Chi University of Technology, New Taipei City 243, Taiwan
[f] Department of Chemical and Materials Engineering, Chang Gung University, Taoyuan 33302, Taiwan
[g] Department of Physics, National Chung Hsing University, Taichung 402, Taiwan

ARTICLE INFO

Keywords:
Alzheimer's disease
Magneto-plasmonic nanoparticle
Faraday effect
Biochip
MiRNA-135a-5p

ABSTRACT

In this study, we present a highly sensitive genoassay for the early detection of Alzheimer's disease (AD) by targeting the microRNA biomarker miRNA-135a-5p. The assay is based on a sandwich hybridization format, utilizing magneto-plasmonic nanoparticles (MPNs) as the detection platform. The concentration of miRNA-135a-5p is directly correlated with the MPN binding events, which are quantitatively measured by monitoring the Faraday rotation angle. Our method demonstrated a remarkable limit of detection (LOD) of 27.1 aM, with a total assay time of 2 h. We validated our method with 13 healthy individuals, 13 individuals with mild cognitive impairment (MCI), and 13 individuals with AD, all of whom underwent neuropsychological diagnosis. Importantly, miRNA-135a-5p levels were measured directly from serum with no further microRNA extraction processing. Statistically significant differences in miRNA-135a-5p levels were observed between the groups, with AD patients showing significantly elevated levels compared to MCI ($p < 10^{-4}$) and healthy controls ($p < 10^{-9}$). MCI individuals also exhibited higher levels compared to healthy controls ($p < 10^{-6}$). Receiver operating characteristic (ROC) analysis demonstrated that our method effectively differentiates between these groups. Specifically, a miRNA-135a-5p concentration below 4.08×10^{-6} nM indicates a healthy individual, while a concentration above 5.68×10^{-4} nM suggests an AD diagnosis. Additionally, no significant correlation was found between age and miRNA-135a-5p levels. Our method offers a highly sensitive and rapid approach for detecting miRNA-135a-5p in patient serum, showcasing the substantial potential to enhance clinical practices in the early diagnosis of AD.

1. Introduction

Alzheimer's disease (AD) accounts for the most of dementia cases and it is perceived by the World Health Organization (WHO) to be a major public health problem [1,2]. The disease has both direct healthcare expenditures and indirect costs like lost productivity from patients and caregivers, which places a significant economic burden on society. It is estimated that the number of people with this condition could rise sharply above 70 million worldwide by 2030 [3]. If there are no breakthroughs in its treatment, the cost could soar making millions of people helpless and overstretching health and social care systems [4,5].

AD is a highly intricate neurodegenerative disorder characterized by progressive cognitive function impairment as well as memory loss. AD starts with an asymptomatic stage proceeding to mild cognitive impairment before finally culminating into full-blown AD [6]. The exact cause of AD is not fully understood, but it is believed to result from a combination of genetic, environmental, and lifestyle factors [7–9]. The accumulation of amyloid-beta plaques and tau tangles in the brain is

* Correspondence to: 250, Kuo Kuang Rd., Taichung 402, Taiwan.
E-mail addresses: huangyc@mail.mcut.edu.tw (Y.-C. Huang), klchen@phys.nchu.edu.tw (K.-L. Chen).

https://doi.org/10.1016/j.snb.2024.137134
Received 24 October 2024; Received in revised form 9 December 2024; Accepted 13 December 2024
Available online 16 December 2024

believed to be the primary cause of AD [10,11]. Genetic predispositions, such as mutations in the Presenilin 1 and 2 genes [12], amyloid precursor protein (APP), and Apolipoprotein E (ApoE) [13], often lead to the production of abnormal amyloid-beta protein (Aβ) [14]. Mutations in the microtubule-associated protein tau (MAPT) gene result in the production of abnormal tau proteins that aggregate into neurofibrillary tangles [15]. Additionally, oxidative stress, inflammation, and impaired neurotransmission have also been implicated in the pathogenesis of AD [16]. The treatment for AD has seen advancements in recent years. Primary therapeutic approaches involve FDA-approved drugs like acetylcholinesterase inhibitors (e.g., donepezil, galantamine, and rivastigmine) and NMDA receptor antagonists (e.g., memantine), that aim at enhancing neurotransmitter function thus alleviating symptoms [17]. However, despite their symptomatic benefits, these medications do not offer a cure as they do not address the underlying neurodegeneration [18,19]. Other therapies like β-site of amyloid precursor protein cleavage enzyme 1 (BACE1) inhibitors prevent the production of amyloid-beta peptides, while Tau-targeting therapies are about preventing tau protein abnormalities [20,21]. Similarly, miRNA replacement therapies could potentially regulate gene expression changes associated with AD [22]. Based on the current situations, the role of early diagnosis is becoming more important. It provides a critical window for therapeutic intervention, which may delay or prevent the onset of severe symptoms [23].

Biosensors are devices that can detect and quantify biomarkers by transforming biological reactions into quantifiable signals using transducer principles. One of the primary advantages of biosensors is their ability to detect low concentrations of analytes, allowing for timely diagnosis and action. Biomarkers are biological indicators that reflect various aspects of disease pathology. In AD, they include the accumulation of amyloid-beta (Aβ) plaques, tau protein tangles, and neuronal loss or dysfunction [24]. Imaging biomarkers such as positron emission tomography (PET), can reveal the density and distribution of plaques using amyloid and tau tracers [25]. Magnetic resonance imaging (MRI) provides detailed images of brain structure, highlighting regions like the hippocampus where atrophy is pronounced [26]. However, these imaging techniques are expensive. Fluid biomarkers, found in cerebrospinal fluid (CSF) and blood, can offer a more cost-effective alternative. CSF biomarkers, including Aβ42/Aβ40 ratio, total tau (t-tau), and phosphorylated tau (p-tau), reflect the presence of neurofibrillary tangles and neuronal injury [27]. Blood-based biomarkers, such as plasma Aβ42/Aβ40, plasma tau, and neurofilament light (NfL) chain, offer less invasive alternatives for detecting amyloid pathology and neurodegeneration [28–30]. Recently, microRNAs (miRNAs) have emerged as promising biomarkers for AD [31]. These small, non-coding RNA molecules play a critical role in regulating gene expression and are deeply involved in the pathological processes of AD [32]. They influence the formation of amyloid-beta plaques, tau tangles, and neuroinflammation [33]. For instance, the miRNA-29 family, including miRNA-29a, miRNA-29b, and miRNA-29c, regulates BACE1 expression. MiRNA-137 is a key regulator of neuronal development and cognitive function. MiRNA-132 and miRNA-212 play a role in the regulation of Tau protein [34]. They have also been found to be dysregulated in the brains, blood, and cerebrospinal fluid, offering potential as biomarkers for AD diagnosis [24,35]. Meanwhile, exosomal miRNAs (exo-miRNAs) have also gained attention. They are enclosed within exosomes, which are small vesicles with a lipid bilayer membrane. This membrane protects miRNAs from degradation by enzymes in the blood and other bodily fluids, making exo-miRNAs stable and reliable for diagnostic purposes [36–38]. In the context of AD, exo-miRNAs derived from neurons, astrocytes, and other brain cells can reflect the pathological state of the brain by mediating intercellular communication and transferring pathological proteins. Studies have demonstrated that certain exo-miRNAs such as miRNA-125b, miRNA-29b, and miRNA-146a are differentially expressed in the body fluid of patients [36,39]. MiRNAs have promising potential as biomarkers for AD, but their biological variability complicates interpretation. Besides, exo-miRNA assays encounter difficulties with exosome isolation methods, which frequently result in low recovery rates or high contamination with free miRNAs. On the other hand, the trajectories of AD biomarkers vary significantly depending on the pathological stage [40]. The alterations in the biomarkers can be very subtle in their early stages, requiring highly sensitive methods for detection. This highlights the necessity for advanced diagnostic tools. Recent research on detecting miRNAs has demonstrated limits of detection (LOD) typically ranging from femtomolar (fM) to attomolar (aM) [37,41]. However, some of these methods are expensive, complex, or time-consuming. To meet the REASSURED diagnostic criteria [42], the development of reliable detection methods and the exploration of robust RNA biomarkers are now critical focal points in the advancement of diagnostic technologies. A comparison of the AD detection methods with our approach is discussed later in the results section.

In this work, we propose a biosensing platform for AD assay utilizing miRNA-135a-5p as a biomarker. Previous studies have indicated that miRNA-135a-5p is upregulated in the serum exosomes of AD patients [43,44]. Furthermore, recent research by Zheng et al. suggested that miRNA-135a-5p plays a crucial role in maintaining synaptic plasticity through its regulation by the transcription factor Foxd3, which controls the expression of Rock2 and thereby influences dendritic spine density and maturity [45]. The dysregulation of miRNA-135a-5p can lead to synaptic and memory impairments, mediated by an increase in Rock2 activity and subsequent phosphorylation of Adducin1. This phosphorylation disrupts synaptic structure, contributing to the cognitive decline observed in AD. However, specific quantification was not detailed; therefore, we aimed to focus on miRNA-135a-5p as a specific blood biomarker for the early detection of AD.

In our previous research, we developed a biosensing platform that utilized the magneto-optical Faraday effect of magneto-plasmonic nanoparticles (MPNs) for protein detection [46,47]. This system was capable of detecting tau protein in plasma with a limit of detection (LOD) of 9 pg/mL [48]. While our earlier work focused on immunoassays and protein targets, this study represents a significant advancement by transitioning to a sandwich-based genoassay for RNA detection. Specifically, we now target miRNA using a biochip format for early detection of AD. Besides, we have integrated an auto-balanced photodetector to further enhance the sensitivity and precision. Due to the stability, lower cost, and specificity of ssDNA-135a-5p, we utilized it to establish the calibration line, achieving an LOD of 27.1 aM. Subsequent testing with clinical serum samples from AD patients successfully targeted miRNA-135a-5p and differentiated its levels between healthy individuals, those with mild cognitive impairment (MCI), and AD patients. Notably, our method does not require complex RNA processing, allowing for rapid test results within 2 h. These findings highlight the potential of our approach for nucleic acid detection and the use of miRNA-135a-5p as a biomarker for early diagnosis of AD.

2. Experimental section

2.1. Synthesis of Fe_3O_4@PEI@Au nanoparticles and preparation of biochips

We utilized core-shell Fe_3O_4@PEI@Au MPNs as the recognition elements in a sandwich genoassay biochip. The synthesis of these MPNs and the detailed biochip fabrication process are outlined in the supplementary material.

2.2. Design of probes for miRNA-135a-5p detection

In this study, we also aimed to validate miRNA-135a-5p as a biomarker for AD. As illustrated in Fig. 1, DNA probes were employed for detection due to their superior chemical stability compared to RNA, which is more prone to hydrolysis and environmental degradation. Additionally, single-stranded DNA-135a-5p (ssDNA-135a-5p)

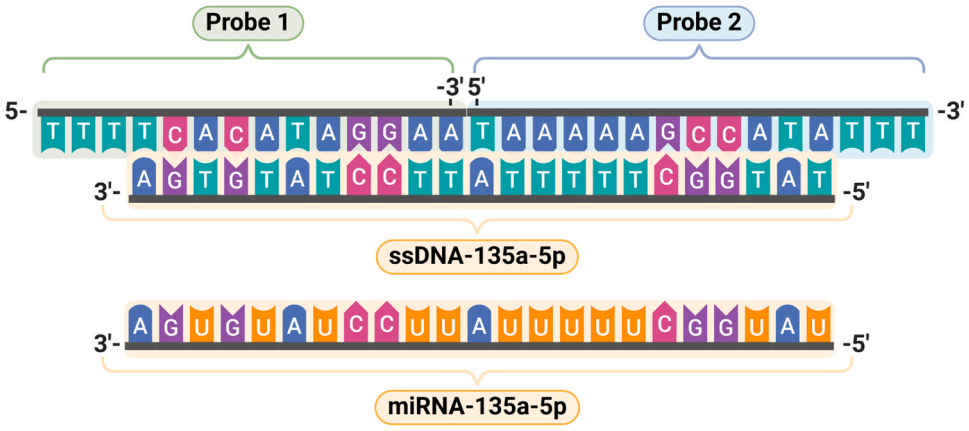

Fig. 1. Sequences of the probes designed for miRNA-135a-5p detection.

corresponding to miRNA-135a-5p was used for calibration purposes. The limitations associated with using DNA in this context are discussed in detail later in the manuscript. It should be noted that while DNA was employed for probe design and calibration, the specific RNA target (miRNA-135a-5p) remained the focus of clinical testing. Consequently, all subsequent discussions and experiments focus solely on the miRNA target.

Two thiol-modified probes were specifically designed for the detection of miRNA-135a-5p, each complementary to distinct sequences of the ssDNA-135a-5p to ensure specificity as shown in Fig. 1. Probe 1 is thiol-modified and engineered to be anchored onto the surface of the biochip. This probe is designed to hybridize with one end of the miRNA sequence. Conversely, Probe 2 is also thiol-modified and is functionalized onto the surface of Fe_3O_4@PEI@Au MPNs. The second probe can hybridize with the opposite end. Together, these two probes facilitate the accurate and specific detection. During the assay, the ssDNA-135a-5p (calibration)/miRNA-135a-5p (clinical test) is first exposed to the Fe_3O_4@PEI@Au MPNs, which allows its one end to bind with Probe 2 on the MPNs. Subsequently, the complex is incubated with the biochip, enabling the other end molecule to pair with Probe 1, thereby anchoring MPNs to the biochip. Both probes were purchased from commercial suppliers and the preparation of the biochip with Probe 1 and the Fe_3O_4@PEI@Au-Probe 2 reagents are detailed in the supplementary material.

2.3. Protocol for detecting ssDNA-135a-5p (calibration)/miRNA-135a-5p (clinical test)

For ssDNA-135a-5p (calibration)/miRNA-135a-5p (clinical test) detection, the sample solution was first incubated with the prepared Fe_3O_4@PEI@Au-Probe 2 reagents at 55 °C for 1 h. The functionalized biochip was then exposed to this mixture under the same conditions. Post incubation, the unbound target and Fe_3O_4@PEI @Au-Probe 2 were washed away with TE buffer and the substrate was dried with nitrogen, finalizing the biochip preparation for measurement. TE buffer solutions were prepared using 40 mM Tris-HCl and 2 mM EDTA at pH 7.4.

2.4. Mechanism of the assay

As mentioned earlier, we employed a sandwich assay using specially designed probes. The probe-target interaction through simple base pairing. This enables the capture of the target miRNA on the biochip, which is integrated with a detection medium consisting of Fe_3O_4@-PEI@Au MPNs. As the concentration of the target analyte increases, so does the accumulation of Fe_3O_4@PEI@Au MPNs on the biochip. When subjected to an external magnetic field, these nanoparticles aggregate and align with the field, enhancing the birefringence effect and amplifying the Faraday rotation phenomenon. Consequently, the concentration of the analyte can be quantitatively determined by measuring the variation of the Faraday rotation angle $\Delta\theta$ of the biochip. The $\Delta\theta$ is defined as the change in the Faraday rotation angle resulting from the binding of MPNs. It is calculated as the difference between the Faraday rotation angle of the biochip after the assay (θ) and the blank biochip before the assay (θ_0): $\Delta\theta = \theta - \theta_0$.

Additionally, the Faraday optical activity of DNA/RNA in the presence of small magnetic fields is negligible, which effectively minimizes background interference and boosts the signal-to-noise ratio. This high specificity ensures that the signals measured are solely attributable to the Fe_3O_4@PEI@Au nanoparticles bound to the target, directly quantifying miRNA-135a-5p levels. Fig. 2 provides a detailed schematic of the experimental setup and workflow.

2.5. Measurement system for Faraday rotation

The experimental setup, depicted in Fig. 3, is a custom-built Faraday rotation analyzer that utilizes a differential detection method to enhance accuracy and stability. A 532 nm single longitudinal mode laser was used, producing a laser beam with a diameter of 0.51 cm and a power output of 1 mW, as measured on the sample. The laser beam is first polarized to produce linearly polarized light, which then passes through the sample located within a custom-built coil. To optimize detection sensitivity, the magnetic field is modulated by a lock-in amplifier. The lock-in amplifier (SR830, Stanford Research Systems, Inc.) drives an amplifier (LVC2016, AE Techron, Inc.), which powers the coil to generate a sinusoidal AC magnetic field of 100 gauss at 813 Hz, chosen for its low-noise characteristics in our experimental environment. The frequency employed in our experiments is far below the thresholds for both Néel and Brownian relaxation, and the applied field is sufficiently small to avoid any heating effects. Furthermore, temperature monitoring during the experiments detected no evidence of heating. After interacting with the sample, the light passes through a half-wave plate to adjust the polarization splitting ratio before entering a Wollaston prism, which splits the light into two orthogonal polarization components. These beams are subsequently detected by an auto-balancing photodetector, where the differential detection technique reduces common-mode noise, enhancing the signal-to-noise ratio for more accurate measurements. The signals are then processed by the lock-in amplifier and recorded digitally for the quantification of the Faraday effect. Under the low-field AC conditions, the Faraday angle can be derived from the ratio of AC to DC signals [46,49]. We employed both lock-in techniques and differential detection with an auto-balanced photodetector to optimize the sensitivity of our platform. Then, the Faraday rotation angle of the biochips can be measured, and the change in the Faraday angle induced by the target can be utilized to quantify the detection.

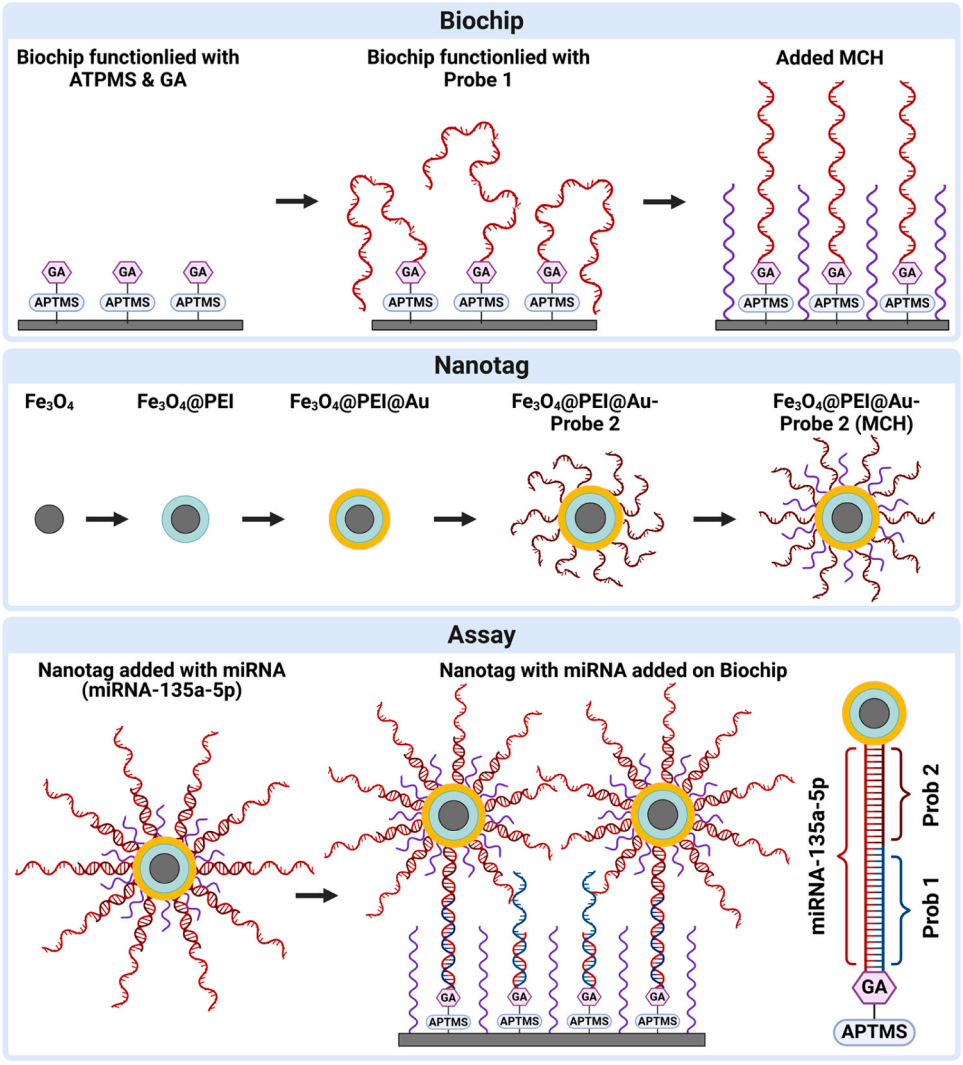

Fig. 2. Flowchart of the sandwich genoassay biochip (Created with Biorender.com).

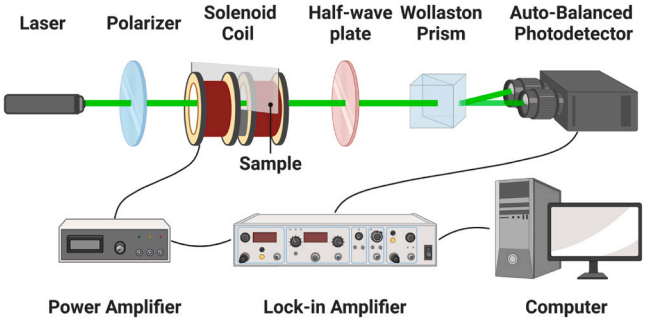

Fig. 3. Schematic diagram of the auto-balancing magneto-optical Faraday effect detection system (Created with Biorender.com).

3. Results and discussions

3.1. Characterization

Transmission electron microscope (TEM) analysis of Fe_3O_4@PEI@Au MPNs revealed uniformly spherical nanoparticles with an average diameter of 200 nm. Lattice fringes corresponding to Fe_3O_4 (220) in the center and Au (311) in the shell of the nanoparticle clearly delineate the core-shell structure [50]. Additionally, the selected area electron diffraction (SAED) patterns showed distinct rings corresponding to multiple crystallographic planes of Fe_3O_4 and Au, confirming the crystallinity of both magnetite and gold in the nanoparticles [51]. TEM images are provided in the supplementary material.

Fig. 4 presents the Energy-Dispersive X-ray Spectroscopy (EDS) analysis of Fe_3O_4@PEI@Au MPNs. The top panel features the scanning electron microscope (SEM) image of the MPNs with a highlighted region chosen for EDS analysis. Subsequent panels display the EDS maps, with each color representing a unique element in which iron is depicted in gray, oxygen in cyan, carbon in red, and gold in yellow. These maps provide a visualization of the spatial distribution of each element within the MPNs. The bottom panel shows the EDS spectroscopy of MPNs, demonstrating the elemental composition of iron, oxygen, carbon, nitrogen, and gold. The EDS maps of these elements indicate the presence of the Fe_3O_4 core, the PEI coating, and the gold shell. The distribution of Fe and O elements is more concentrated in the core of the particles, whereas the C and Au elements are predominantly found on the surface. They also reveal a uniform distribution of elements across the MPNs, affirming the effectiveness of our synthesis. These characterization results conclusively demonstrate the successful synthesis of the Fe_3O_4@PEI@Au MPNs, as evidenced by the consistency with the intended design.

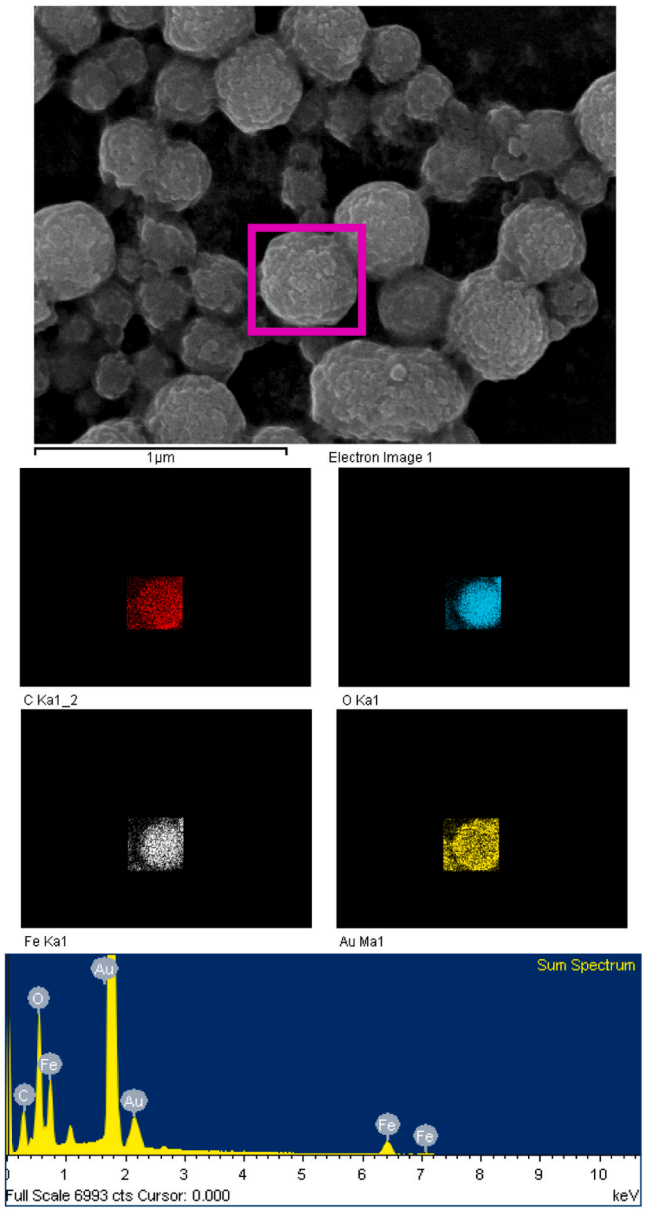

Fig. 4. EDS analysis of Fe_3O_4@PEI@Au MPNs.

3.2. Calibration curve established by ssDNA-135a-5p

For quantification, we established a calibration curve using the ssDNA-135a-5p with various concentrations ranging from 100 nM to 10^{-10} nM, diluted using TE buffer. We monitor the changes in Faraday rotation angle $\Delta\theta$ of the biochips treated with different concentrations of ssDNA-135a-5p. To obtain the variation caused by the target analytes, the baseline Faraday rotation angle of the clean biochip (θ_0) was measured prior to testing and subtracted from the experimental readings. Each concentration was measured five times within a span of two minutes, with each measurement representing the average of 100 readings. These five values were then averaged to represent the measurement for each concentration. We conducted experiments in triplicate using different batches of reagents and biochips to ensure the consistency and reliability. Fig. 5a illustrates the relationship between $\Delta\theta$ and logarithmic concentration of ssDNA135a-5p. Each data point represents the averaged $\Delta\theta$ with error bars indicating the standard error derived from triplicate experiments. The data shows good linearity, as depicted by the red fitting curve in Fig. 5a. The linear fit indicates a positive correlation between $\Delta\theta$ and the logarithmic concentration, with an excellent R^2 value of 0.99. As previously detailed, our measurements were conducted over a 2-minute duration. Repeatability was assessed by analyzing the deviation values of these readings. Reproducibility was evaluated by analyzing the results among triplicate experiments. Fig. 5b demonstrates the statistical results of the repeated measurements and reproduced measurements of $\Delta\theta$ for different concentrations, indicated by light orange and light green, respectively. The bars represent the average values with their deviations. Fig. 5c highlights the deviation values for repeatability and reproducibility. For all tested concentrations, the repeated measurements remained stable over time. The deviations were consistently within 2 µrad, highlighting the repeatability of the biochip. Triplicate experiments were conducted using three distinct biochips, each fabricated and tested on separate days. Besides, both deviations seem to be stable and independent of the concentration, which could indicate that the noise is not influenced by the sample concentration. Consistency in noise could indicate the accuracy of our measurements, as it ensures that the data reflects true variations in the sample rather than being confounded by variable noise levels. The average deviations across different concentrations for repeatability and reproducibility were 0.645 and 1.080 µrad, respectively, as indicated by the orange dotted line and green dashed line in Fig. 5c. The smaller deviation in repeatability compared to reproducibility is reasonable, due to a broader range of potential influences on the measurement. The overall consistency in the data validates our biochips' reliability for quantitative analysis.

Besides, the limit of detection was determined by the conventional method $3.3\sigma/S$, where σ is the standard deviation of the response and S is the slope of the calibration line. Here, σ represents the standard deviation of the blank samples, which is 0.676 µrad. The blank sample in our work refers to the biochip that has undergone the entire process without the addition of the analyte. The deviation of the blank samples is comparable to the average deviations observed in repeatability and reproducibility tests, providing a convincing validation of the results. Consequently, the LOD of our system can be estimated to be 27.1 aM, demonstrating the high sensitivity of our method.

The $\Delta\theta$ is described by $\Delta\theta = kMl$, where k is a proportionality constant, l is the optical path length, and M represents the magnetization. The magnetization M from MPNs is directly proportional to its number bound to the biochip. Furthermore, the correlation between analyte concentration and the number of bound MPNs can be described by the Hill equation, which characterizes the binding behavior of analytes to receptors, resulting in a logarithmic dependence of $\Delta\theta$ on concentration. However, our results reveal a linear relationship between the $\Delta\theta$ and the logarithm of concentration. We attribute this linearity to the sensor operating within the linear region of the binding curve, as the calibration concentrations used were below the saturation threshold.

3.3. Mutation DNA detection

To affirm the reliability and specificity of our method as shown in Fig. 5d, we conducted a series of mismatch detection tests. Fig. 5e illustrates the testing sequences of ssDNA-135a-5p and its three mismatch scenarios: a single-base mismatch (Target 1, where Cytosine is replaced by Adenine), a double-base mismatch (Target 2, with two Cytosine replaced by two Adenine), and a triple-base mismatch (Target 3, featuring sequential replacements of Cytosine, Cytosine and Thymine with Adenine, Adenine, and Cytosine, respectively). All samples were prepared at a low concentration of 0.01 nM to reflect typical assay conditions. Fig. 5d illustrates the changes in Faraday rotation angle $\Delta\theta$ for detecting these samples. The results reveal a significantly higher response of 15.94 µrad for the target ssDNA-135a-5p compared to much lower responses for mismatched DNA sequences—specifically, 2.43 µrad for one mismatch, 1.21 µrad for two, and 0.47 µrad for three. This decrease not only underscores the method's specificity but also effectively distinguishes between similar, non-identical sequences. The

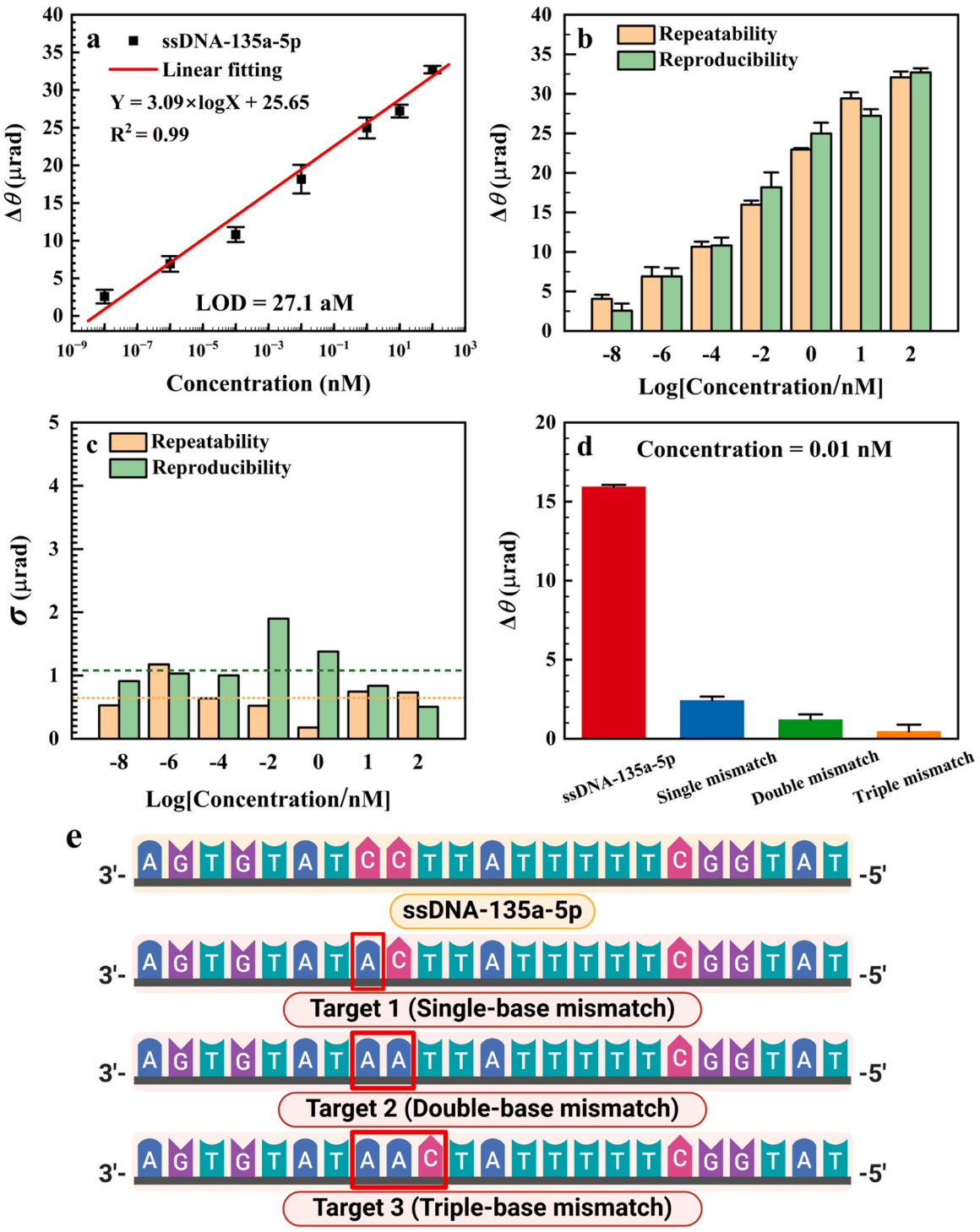

Fig. 5. (a) Faraday rotation angle changes $\Delta\theta$ of biochips with different concentrations of ssDNA-135a-5p. The blue line represents the minimum detectable signal strength, and the red line represents the fitting logistic curve. (b) Bar plots of $\Delta\theta$ and (c) Bar plots of the deviation of $\Delta\theta$ for biochips with different concentrations of ssDNA-135a-5p from repeatability and reproducibility measurements. (d) Faraday rotation angle changes $\Delta\theta$ of biochips with ssDNA having different mismatch sites and (e) ssDNA sequence diagrams of different mismatch sites.

reduction in response to an increasing number of mismatches corresponds with the anticipated decrease in binding affinity.

3.4. Assays Comparison

Detection of miRNA has recently been advanced to show its potential for diagnosing AD. Several studies have identified miRNAs as possible biomarkers. Delkhahi et al. developed a gold nanoparticle-based colorimetric assay for the detection of miRNA-137. This approach employs the hybridization chain reaction (HCR) amplification technique, achieving a LOD of 0.25 nM [52]. Pan et al. introduced a dual electrode sensing surface using gold nanourchins as electrochemical signal amplifiers that had an LOD of 0.01 pM for miRNA-137 [53]. Miglione et al. developed electrochemical strips for detecting miRNA-29a, with an LOD of 1 nM for DNA-based targets and 0.15 nM for RNA-based targets within a duration of 3 h [54]. Lim et al. proposed a hydrogel-based

sensor for detecting miRNA-574-5p. This sensor is capable of self-signal amplification and achieves an LOD of 1.29 pM for DNA-based targets and 1.23 pM for RNA-based targets within 2 h[55]. Khalilzadeh et al. developed an electrochemical biosensor for miRNA-146a, achieving an LOD of 10 pM over 4 h [56]. Compared to other methods that typically detect miRNA biomarkers at pM levels within a few h, our technique achieves an LOD of 27.1 aM within 2 h. The improvement in sensitivity suggests earlier and more accurate detection of AD. Besides, our method does not require complicated fabrication or pre-processing steps, making it more practical and accessible. We have conducted clinical tests to validate the effectiveness and reliability of our method, as discussed below. The summary of these biosensors for AD is listed in Table 1.

3.5. Clinical tests

The clinical research was conducted following approval from the Institutional Review Board (IRB), under case number CE22366A, in collaboration with Taichung Veterans General Hospital. A total of 39 clinical serum samples were obtained from participants, all of whom were required to be at least 50 years old. The participants were categorized into three demographic groups for analysis: 13 healthy individuals, 13 subjects with mild cognitive impairment (MCI), and 13 patients diagnosed with AD. Healthy control group participants were selected on the basis that they had no history of dementia, cognitive impairment, or neurological disorders. All participants underwent comprehensive neuropsychological assessments conducted by neurologists in the hospital. These assessments included the Mini-Mental State Examination (MMSE) [57], the Clinical Dementia Rating (CDR) [58], and the Cognitive Abilities Screening Instrument (CASI) [59]. The age distribution within the healthy cohort averaged 66 ± 8 years, including six males with an average age of 69 ± 6 years and seven females averaging 63 ± 4 years. The MCI group had an average age of 73 ± 5 years, with seven males averaging 74 ± 3 years and six females averaging 72 ± 4 years. In the AD category, the average age was calculated at 69 ± 8 years, where the male participants averaged 72 ± 8 years and the female participants 78 ± 5 years. Details of the assessments and sample collections for participants are listed in the supplementary material.

Fig. 6 illustrates the logarithmic concentration of miRNA-135a-5p among three distinct groups: AD patients, individuals with MCI, and healthy controls. The box plot indicates a statistically significant increase in the log-transformed levels of miRNA-135a-5p in AD patients compared to MCI individuals ($*p < 10^{-4}$), as determined by a one-tailed *t*-test, and healthy controls ($***p < 10^{-9}$). The MCI individuals also show a significant difference when compared to healthy controls ($**p < 10^{-6}$). Using the Receiver Operating Characteristic (ROC) analysis detailed in Fig. 7, we can establish specific cutoff points: 4.08×10^{-6} nM for distinguishing between healthy and MCI individuals, and 5.68×10^{-4} nM for differentiating MCI from AD patients. The red dashed lines in Fig. 6 mark the threshold levels for each comparison. The data suggest that miRNA-135a-5p could potentially serve as a biomarker for differentiating between stages of cognitive impairment, with elevated levels correlating with the severity of the condition.

To further assess the diagnostic precision of our method, ROC curves were employed. Fig. 7 illustrates the diagnostic accuracy of our method

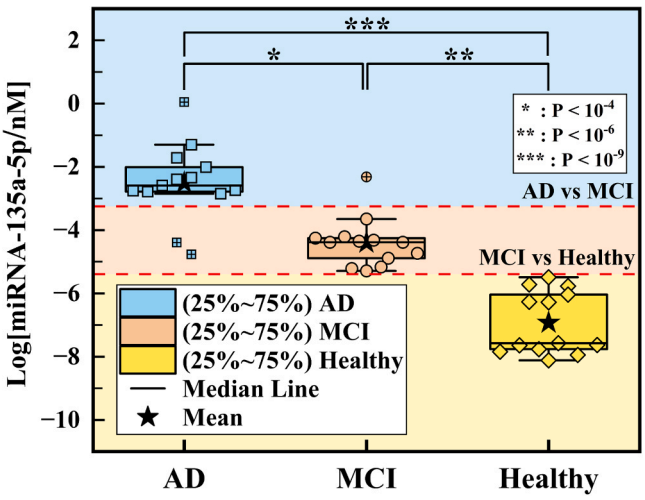

Fig. 6. Box-and-whisker plots illustrating the logarithmic concentration of miRNA-135a-5p in individuals with AD, MCI, and in healthy controls. The statistical significance of differences between groups is indicated by asterisks: * denotes $p < 10^{-4}$, * * denotes $p < 10^{-6}$ and * ** denotes $p < 10^{-9}$. The red dashed lines represent the threshold levels for distinguishing between AD and MCI, and MCI and healthy controls. Points marked with a cross represent outliers.

with miRNA-135a-5p as a biomarker through ROC curves. The area under the curve (AUC) values effectively demonstrates the precision in differentiating cognitive states: healthy versus MCI (AUC= 1), AD versus MCI (AUC= 0.86), and AD versus healthy (AUC= 1). A combined comparison of healthy versus AD and MCI also yields a perfect AUC of 1. These results, with high AUC values across different group comparisons, indicate that our method has an excellent discriminatory ability to distinguish between healthy individuals, those with MCI, and those with AD. This confirms a reliable diagnostic capability for our method targeting miRNA-135a-5p, particularly in distinguishing healthy individuals from those with cognitive impairments, with slightly less distinction between MCI and AD cases. We have established a framework to examine how miRNA-135a-5p biomarkers correlate with stages of AD. Our method is well-positioned to identify miRNA-135a-5p biomarkers that could signify the transition from normal cognitive function to MCI and eventually AD. This approach could ultimately lead to more effective diagnostic tools and treatments for AD.

3.6. Discussion

By incorporating the Faraday rotation measurement, we have demonstrated a new pathway for miRNA detection that leverages the unique properties of magneto-plasmonic nanoparticles, providing an innovative alternative to more conventional analytical approaches. Exceptional sensitivity and selectivity were achieved through the integration of gold-shell MPNs, an auto-balanced detector, and a lock-in amplification technique. This approach significantly enhances the assay's performance, enabling the detection of aM concentrations.

Table 1
Comparison of miRNA detection methods for AD.

Method	Target	LOD	Calibration	Usage time	Ref.
Colorimetric detection	miRNA−137	0.25 nM	RNA	2 hr	[52]
Dual electrode sensing surface	miRNA−137	0.01 pM	RNA	N/A	[53]
Electrochemical strips	miRNA−29a	1.0 nM	DNA	3 hr	[54]
		0.15 nM	RNA		
Hydrogels-based sensor	miRNA−574–5p	1.29 pM	DNA	2 hr	[55]
		1.23 pM	RNA		
Electrochemical genosensor	miRNA−146a	10 pM	RNA	4 hr	[56]
This work	miRNA−135a−5p	27.10 aM	DNA	2 hr	-

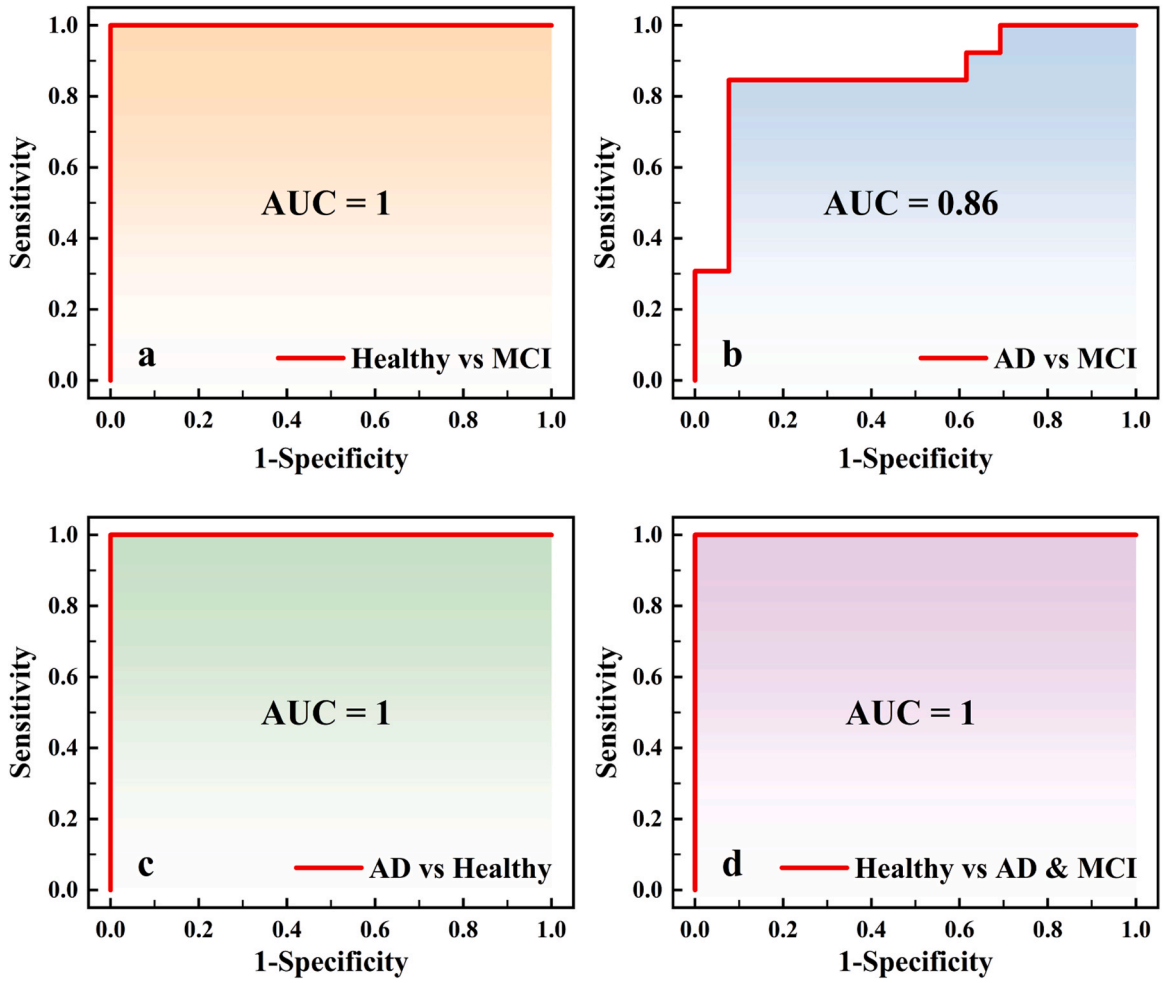

Fig. 7. ROC curves comparing the diagnostic performance for (a) Healthy vs. MCI, (b) AD vs. MCI, (c) AD vs. Healthy, and (d) Healthy vs. AD+MCI groups. The AUC is provided for each comparison, with AUC= 1 indicating perfect diagnostic ability and AUC= 0.86 indicating high diagnostic ability.

Furthermore, results of clinical trial using our methods suggest that our detection approach targeting biomarker miRNA-135a-5p aligns with doctors' diagnoses and can effectively distinguish different stages of AD. However, there are still challenges to address and overcome in terms of assay optimization and validation for broader clinical use.

When establishing the calibration curve, we used ssDNA, which slightly differs from the actual RNA targets in serum samples. This choice was originally made due to the higher stability of DNA compared to RNA, as well as its economic advantages. Differences in binding affinity between DNA/DNA and DNA/RNA hybrids could potentially affect detection, introducing deviation and causing discrepancies in the actual concentration when detecting RNA. However, our results can still serve as a reliable reference since this deviation is systematic. Additionally, because the target is miRNA, which is a short sequence, the differences between DNA/DNA and DNA/RNA binding are likely minimal. Therefore, we believe that the quantity and variations should not significantly influence the outcome. Moreover, unlike orthodox methods that involve isolating and extracting RNA from exosomes, we directly measured circulating free miRNA-135a-5p in patient serum samples with genoassays. Although we did not implement specific measures to prevent RNA degradation, our clinical trial results demonstrated significant statistical differences among AD, MCI, and healthy controls. The ROC curve also indicated a strong discriminatory capability. Our results align with neuropsychological assessments and are consistent with other research findings [43,44]. We hypothesize that despite the inherent fragility and susceptibility of RNA to degradation, the miRNA-135a-5p, being a smaller fragment of RNA, might be less prone to such changes, enhancing its stability during sample collection and assays. It could also be released from exosomes into the blood, making direct detection feasible without the need for additional exosome processing. We also found that miRNA-135a-5p could serve as an age-independent biomarker for AD. As shown in Fig. 8, the correlation between age

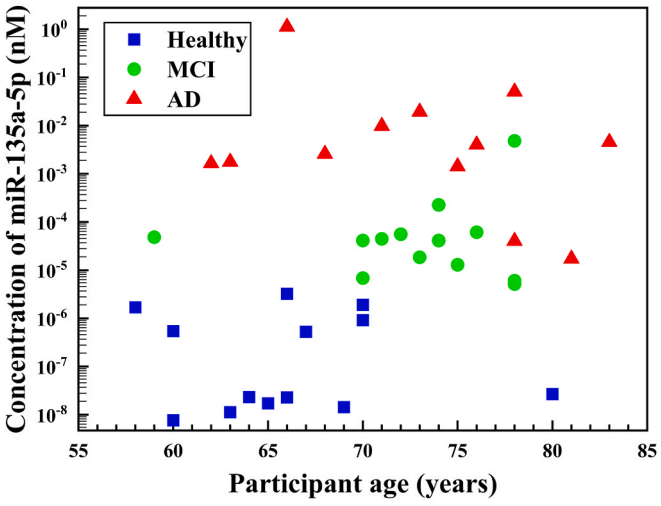

Fig. 8. The relationship between the logarithmic concentration of miRNA-135a-5p and the age of participants.

and logarithmic miRNA-135a-5p concentration across different groups (Healthy, MCI, and AD) shows no obvious correlation. We analyzed each group using Pearson, Spearman, and Kendall correlation methods, as listed in Table 2. All three methods consistently showed weak or small correlations across the three groups. Moreover, since the p-values are far above the common significance threshold of 0.05, we cannot reject the null hypothesis. Consequently, we infer that there is no significant correlation between age and the logarithmic concentration of miRNA-135a-5p.

Additionally, we have observed differential expression of miRNA-135a-5p in our work compared to the findings reported by other studies [45]. Specifically, miRNA-135a-5p levels increased in the blood, while levels decreased in the frontal cortex of AD patients. Why the concentration of miRNA-135a-5p increases in the blood as AD progresses, while it decreases in hippocampal neurons is not yet clear. We hypothesize that some factors may cause miRNA-135a-5p to be expelled extracellularly into the bloodstream, leading to a decrease in miRNA-135a-5p levels within brain neurons and thereby contributing to the progression of AD. However, the precise mechanisms underlying these changes of miRNA-135a-5p levels in the blood and brain neurons require further investigation. Besides, this study focuses on miRNA-135a-5p for the diagnosis of AD. While the results indicate high sensitivity and selectivity, further research is necessary. Future research could conduct parallel tests of miRNA-135a-5p alongside other well-established AD biomarkers, such as amyloid-beta and tau proteins. These comparative studies could provide a better understanding of the diagnostic role of miRNA-135a-5p within the broader context of AD biomarker research, further enhancing its clinical relevance.

4. Conclusion

We have developed a highly sensitive platform for the early detection of AD by integrating a sandwich genoassay with magnetoplasmonic nanoparticles (MPNs), leveraging their magneto-optical properties. We designed two thiolate probes, Probe 1 and Probe 2, specifically targeting miRNA-135a-5p to facilitate the sandwich assay. The miRNA-135a-5p concentration is proportional to the binding of the MPNs on the biochip and can be transduced into a measurable signal using the Faraday effect. With our signal-to-noise ratio enhanced Faraday measurement setup, our system demonstrated both good reproducibility among triplicate experiments conducted at three different times and a remarkable LOD of 27.1 aM. Moreover, clinical validation was conducted on 39 participants, divided equally among healthy individuals, people with MCI, and AD patients. We successfully measured the concentration of miRNA-135a-5p in the serum of participants. There was a statistically significant increase in miRNA-135a-5p levels in individuals with AD compared to those with MCI ($p < 10^{-6}$) and compared to healthy controls ($p < 10^{-9}$). Additionally, individuals with MCI also had significantly higher miRNA-135a-5p levels compared to healthy controls ($p < 10^{-4}$). Our findings align with clinical diagnoses and indicate that miRNA-135a-5p concentrations in serum below 4.08×10^{-6} nM typically signify healthy individuals, whereas levels exceeding 5.68×10^{-4} nM may indicate AD.

Our method has demonstrated its good sensitivity and reliability through clinical tests. It is time-efficient, with measurements completed within 2 h, and cost-effective, requiring only 3 USD per test. Notably, miRNA-135a-5p may hold potential as a biomarker for AD in clinical applications. Its elevated levels in serum and regulatory roles in AD pathology aid in early diagnosis and provide insights into disease mechanisms. Our experimental conditions and results further indicate that miRNA-135a-5p allows for straightforward detection in blood without the need for complex extraction or preservation processes. Additionally, our findings suggest that miRNA-135a-5p could serve as an age-independent biomarker, enhancing its reliability across diverse patient populations. Overall, our method targeting miRNA-135a-5p meets the critical criteria of a biosensor—sensitivity, specificity, cost-effectiveness, and ease of use—demonstrating promising potential for the diagnosis of AD. However, we acknowledge certain limitations, including the need for further comparison with well-established AD biomarkers, and the current calibration approach could benefit from additional refinements. Nonetheless, the results provide a promising foundation for the novel application of the Faraday effect in RNA detection and reinforce the potential of miRNA-135a-5p as a robust AD biomarker. Future efforts will focus on addressing these limitations to further validate this approach.

Table 2
Correlation coefficients for different participants groups.

Group Correlation type	Healthy (coefficient/p-value)	MCI (coefficient/p-value)	AD (coefficient/p-value)
Pearson	−0.0515/ 0.867	0.0645/0.834	−0.323/0.283
Spearman	0.232/ 0.446	−0.0860/0.780	−0.138/0.654
Kendall	0.170/ 0.425	−0.0534/0.805	−0.0903/0.669

CRediT authorship contribution statement

Yu-Ching Huang: Writing – review & editing, Supervision, Resources, Investigation. **Kuen-Lin Chen:** Writing – review & editing, Writing – original draft, Supervision, Resources, Project administration, Investigation, Formal analysis, Conceptualization. **Chin-Wei Lin:** Writing – original draft, Investigation, Formal analysis. **Jing-Han Huang:** Investigation, Formal analysis. **Po-Han Lin:** Writing – review & editing, Resources, Investigation. **Ting-Bin Chen:** Writing – review & editing, Resources, Investigation. **Li-Min Wang:** Writing – review & editing, Resources, Investigation.

Declaration of Generative AI and AI-Assisted Technologies in the Writing Process

During the preparation of this work the authors used ChatGPT-4 in order to improve readability and language of the work. After using this tool, the authors reviewed and edited the content as needed and take full responsibility for the content of the publication.

Declaration of Competing Interest

The authors declare that they have no known competing financial interests or personal relationships that could have appeared to influence the work reported in this paper

Acknowledgments

The authors would like to acknowledge the support from the National Science and Technology Council of Taiwan (Grant Nos. NSTC 112–2221-E-005–034, NSTC 112–2628-E-131–001-MY4 and NSTC 113–2622-E-131–006) and Taichung Veterans General Hospital/National Chung Hsing University Joint Research Program (Grant No. TCVGH-NCHU-1110121). The authors also thank Biorender.com for providing the tools to better represent the figures. Figs. 1, 2, 3, 5, and the figure abstract were created using Biorender.com.

Appendix A. Supporting information

Supplementary data associated with this article can be found in the online version at doi:10.1016/j.snb.2024.137134.

Data availability

Data will be made available on request.

References

[1] W.H. Organization, Dementia: a public health priority: World Health Organization; 2012.
[2] H. Jindal, B. Bhatt, S. Sk, J.Singh Malik, Alzheimer disease immunotherapeutics: then and now, Hum. Vaccin. Immunother. 10 (2014) 2741–2743.
[3] T. McGill-Carter, Market analysis Alzheimer's disease 2020, J. Psychiatry 22 (2020) 21–22.
[4] F.T. Hane, M. Robinson, B.Y. Lee, O. Bai, Z. Leonenko, M.S. Albert, Recent progress in Alzheimer's disease research, part 3: diagnosis and treatment, J. Alzheimers Dis. 57 (2017) 645–665.
[5] As Association, Alzheimer's disease facts and figures, Alzheimer'S. Dement. 15 (2019) (2019) 321–387.
[6] J. Therriault, E.R. Zimmer, A.L. Benedet, T.A. Pascoal, S. Gauthier, P. Rosa-Neto, Staging of Alzheimer's disease: past, present, and future perspectives, Trends Mol. Med. 28 (2022) 726–741.
[7] Z. Breijyeh, R. Karaman, Comprehensive review on Alzheimer's disease: causes and treatment, Molecules 25 (2020) 5789.
[8] S. Khan, K.H. Barve, M.S. Kumar, Recent advancements in pathogenesis, diagnostics and treatment of Alzheimer's disease, Curr. Neuropharmacol. 18 (2020) 1106–1125.
[9] E. Angelopoulou, Y.N. Paudel, S.G. Papageorgiou, C. Piperi, APOE genotype and Alzheimer's disease: the influence of lifestyle and environmental factors, ACS Chem. Neurosci. 12 (2021) 2749–2764.
[10] H. Ashrafian, E.H. Zadeh, R.H. Khan, Review on Alzheimer's disease: inhibition of amyloid beta and tau tangle formation, Int. J. Biol. Macromol. 167 (2021) 382–394.
[11] A. Atlante, D. Valenti, Mitochondrial complex I and β-amyloid peptide interplay in alzheimer's disease: a critical review of new and old little regarded findings, Int J. Mol. Sci. 24 (2023) 15951.
[12] H. Bae, K.H. Shim, J. Yoo, Y.-S. Yang, S.S.A. An, M.-J. Kang, Double mutations in a patient with early-onset alzheimer's disease in Korea: An APP Val551Met and a PSEN2 His169Asn, Int J. Mol. Sci. 24 (2023) 7446.
[13] M. Abyadeh, V. Gupta, J.A. Paulo, S. Sheriff, S. Shadfar, M. Fitzhenry, et al., Apolipoprotein ε in brain and retinal neurodegenerative diseases, Aging Dis. 14 (2023) 1311.
[14] J. Andrade-Guerrero, A. Santiago-Balmaseda, P. Jeronimo-Aguilar, I. Vargas-Rodríguez, A.R. Cadena-Suárez, C. Sánchez-Garibay, et al., Alzheimer's disease: an updated overview of its genetics, Int. J. Mol. Sci. 24 (2023) 3754.
[15] L. Ritsma, M. Bsibsi, L. Buti, F. Stevenhagen, S.C. Sancerni, E. de Kraa, et al., Development and characterization of a robust in vitro disease cell line to study tauopathies, Alzheimer'S. Dement. 19 (2023) e076621.
[16] N. Cherbuin, E.I. Walsh, L. Leach, A. Bruestle, R. Burns, K.J. Anstey, et al., Elevated oxidative stress and inflammatory levels are associated with plasma AD biomarkers in middle-age, Alzheimer'S. Dement. 19 (2023) e059828.
[17] M. Vaz, S. Silvestre, Alzheimer's disease: Recent treatment strategies, Eur. J. Pharmacol. 887 (2020) 173554.
[18] R. Briggs, S.P. Kennelly, D. O'Neill, Drug treatments in Alzheimer's disease, Clin. Med. 16 (2016) 247–253.
[19] F.R. Buccellato, M. D'Anca, G.M. Tartaglia, M. Del Fabbro, E. Scarpini, D. Galimberti, Treatment of Alzheimer's disease: beyond symptomatic therapies, Int. J. Mol. Sci. 24 (2023) 13900.
[20] F. Iram, M. Shahid, J. Ansari, G.M. Ashraf, M.I. Hassan, A. Islam, Navigating the maze of alzheimer's disease by exploring BACE1: discovery, current scenario, and future prospects, Ageing Res. Rev. (2024) 102342.
[21] E.E. Congdon, C. Ji, A.M. Tetlow, Y. Jiang, E.M. Sigurdsson, Tau-targeting therapies for Alzheimer disease: current status and future directions, Nat. Rev. Neurol. 19 (2023) 715–736.
[22] C.N. Keighron, S. Avazzadeh, K. Goljanek-Whysall, B. McDonagh, L. Howard, T. Ritter, et al., Extracellular vesicles, cell-penetrating peptides and miRNAs as future novel therapeutic interventions for Parkinson's and Alzheimer's disease, Biomedicines 11 (2023) 728.
[23] S. Rani, S.B. Dhar, A. Khajuria, D. Gupta, P.K. Jaiswal, N. Singla, et al., Advanced overview of biomarkers and techniques for early diagnosis of alzheimer's disease, Cell. Mol. Neurobiol. 43 (2023) 2491–2523.
[24] Y.A.R. Mahaman, K.S. Embaye, F. Huang, L. Li, F. Zhu, J.-Z. Wang, et al., Biomarkers used in Alzheimer's disease diagnosis, treatment, and prevention, Ageing Res. Rev. 74 (2022) 101544.
[25] C. Maschio, R. Ni, Amyloid and tau positron emission tomography imaging in Alzheimer's disease and other tauopathies, Front. Aging Neurosci. 14 (2022) 838034.
[26] G. Mukhtar, S. Farhan, Convolutional neural network based prediction of conversion from mild cognitive impairment to alzheimer's disease: a technique using hippocampus extracted from mri, Adv. Electr. Comput. Eng. 20 (2020) 113–122.
[27] D.A. McGrowder, F. Miller, K. Vaz, C. Nwokocha, C. Wilson-Clarke, M. Anderson-Cross, et al., Cerebrospinal fluid biomarkers of Alzheimer's disease: current evidence and future perspectives, Brain Sci. 11 (2021) 215.
[28] S. Janelidze, S. Palmqvist, A. Leuzy, E. Stomrud, I.M. Verberk, H. Zetterberg, et al., Detecting amyloid positivity in early Alzheimer's disease using combinations of plasma Aβ42/Aβ40 and p-tau, Alzheimer'S. Dement. 18 (2022) 283–293.
[29] S. Wang, J. Hall, M. Petersen, S.E. O'Bryant, R. Nandy, The diagnostic performance of plasma amyloid β, total tau and neurofilament light chain levels in mild cognitive impairment and Alzheimer's disease dementia: the health & aging brain among Latino Elders study, Alzheimer'S. Dement. 19 (2023) e074189.
[30] C. Delaby, C. Hirtz, S. Lehmann, Overview of the blood biomarkers in Alzheimer's disease: promises and challenges, Rev. Neurol. 179 (2023) 161–172.
[31] S. Liu, M. Fan, Q. Zheng, S. Hao, L. Yang, Q. Xia, et al., MicroRNAs in Alzheimer's disease: potential diagnostic markers and therapeutic targets, Biomed. Pharm. 148 (2022) 112681.
[32] X. Kou, D. Chen, N. Chen, The regulation of microRNAs in Alzheimer's disease, Front. Neurol. 11 (2020) 524976.
[33] J. Zhao, D. Yue, Y. Zhou, L. Jia, H. Wang, M. Guo, et al., The role of microRNAs in Aβ deposition and tau phosphorylation in Alzheimer's disease, Front. Neurol. 8 (2017) 342.
[34] S. Silvestro, P. Bramanti, E. Mazzon, Role of miRNAs in Alzheimer's disease and possible fields of application, Int. J. Mol. Sci. 20 (2019) 3979.
[35] Y. Zhao, V. Jaber, P.N. Alexandrov, A. Vergallo, S. Lista, H. Hampel, et al., microRNA-based biomarkers in Alzheimer's disease (AD), Front. Neurosci. 14 (2020) 585432.
[36] G.-h Cui, J. Zhu, Y.-c Wang, J. Wu, J.-r Liu, H.-d Guo, Effects of exosomal miRNAs in the diagnosis and treatment of Alzheimer's disease, Mech. Ageing Dev. 200 (2021) 111593.
[37] Y. Wu, Y. Zhang, X. Zhang, S. Luo, X. Yan, Y. Qiu, et al., Research advances for exosomal miRNAs detection in biosensing: from the massive study to the individual study, Biosens. Bioelectron. 177 (2021) 112962.
[38] H. Aheget, L. Mazini, F. Martin, B. Belqat, J.A. Marchal, K. Benabdellah, Exosomes: their role in pathogenesis, diagnosis and treatment of diseases, Cancers 13 (2021) 84.
[39] I. Manna, S. De Benedittis, A. Quattrone, D. Maisano, E. Iaccino, A. Quattrone, Exosomal miRNAs as potential diagnostic biomarkers in Alzheimer's disease, Pharmaceuticals 13 (2020) 243.
[40] K. Blennow, H. Zetterberg, Biomarkers for Alzheimer's disease: current status and prospects for the future, J. Intern. Med. 284 (2018) 643–663.
[41] E. Pishbin, F. Sadri, A. Dehghan, M.J. Kiani, N. Hashemi, I. Zare, et al., Recent advances in isolation and detection of exosomal microRNAs related to Alzheimer's disease, Environ. Res. (2023) 115705.
[42] K.J. Land, D.I. Boeras, X.-S. Chen, A.R. Ramsay, R.W. Peeling, REASSURED diagnostics to inform disease control strategies, strengthen health systems and improve patient outcomes, Nat. Microbiol. 4 (2019) 46–54.
[43] T.T. Yang, C.G. Liu, S.C. Gao, Y. Zhang, P.C. Wang, The serum exosome derived MicroRNA– 135a,– 193b, and– 384 were potential Alzheimer's disease biomarkers, Biomed. Environ. Sci. 31 (2018) 87–96.
[44] C.G. Liu, M. Shuang, L. Ying, L. Yao, Z. Yue, P.C. Wang, MicroRNA-135a in ABCA1-labeled exosome is a serum biomarker candidate for Alzheimer's disease, Biomed. Environ. Sci. 34 (2021) 19–28.
[45] K. Zheng, F. Hu, Y. Zhou, J. Zhang, J. Zheng, C. Lai, et al., miR-135a-5p mediates memory and synaptic impairments via the Rock2/Adducin1 signaling pathway in a mouse model of Alzheimer's disease, Nat. Commun. 12 (2021) 1903.
[46] K.-L. Chen, Y.-S. Lin, J.-M. Chen, C.-H. Wu, C.-C. Jeng, L.-M. Wang, A sensitive platform for in vitro immunoassay based on biofunctionalized magnetic nanoparticles and magneto-optical Faraday effect, Sens Actuators B 258 (2018) 947–951.
[47] C.-W. Lin, J.-M. Chen, Y.-J. Lin, L.-W. Chao, S.-Y. Wei, C.-H. Wu, et al., Magneto-optical characteristics of streptavidin-coated Fe3O4@ Au Core-shell nanoparticles for potential applications on biomedical assays, Sci. Rep. 9 (2019) 16466.
[48] K.-L. Chen, P.-H. Tsai, C.-W. Lin, J.-M. Chen, Y.-J. Lin, P. Kumar, et al., Sensitivity enhancement of magneto-optical Faraday effect immunoassay method based on biofunctionalized γ-Fe2O3@ Au core-shell magneto-plasmonic nanoparticles for the blood detection of Alzheimer's disease, Nanomed. Nanotechnol. Biol. Med. 46 (2022) 102601.
[49] V. Valev, J. Wouters, T. Verbiest, Differential detection for measurements of Faraday rotation by means of ac magnetic fields, Eur. J. Phys. 29 (2008) 1099.
[50] F. Hu, H. Lin, Z. Zhang, F. Liao, M. Shao, Y. Lifshitz, et al., Smart liquid SERS substrates based on Fe3O4/Au nanoparticles with reversibly tunable enhancement factor for practical quantitative detection, Sci. Rep. 4 (2014) 7204.
[51] C. Huang, J. Jiang, C. Muangphat, X. Sun, Y. Hao, Trapping iron oxide into hollow gold nanoparticles, Nanoscale Res Lett. 6 (2011) 1–5.
[52] S. Delkhahi, M. Rahaie, F. Rahimi, Design and fabrication a gold nanoparticle-DNA based nanobiosensor for detection of microRNA involved in Alzheimer's disease, J. Fluoresc. 27 (2017) 603–610.
[53] G. Pan, J. Ji, S. Li, A. Wu, Gold nanourchin enhances detection of Alzheimer's disease biomarker "miRNA-137" on dual electrode sensing surface, Biotechnol. Appl. Biochem. 69 (2022) 2573–2579.
[54] A. Miglione, A. Raucci, J. Amato, S. Marzano, B. Pagano, T. Raia, et al., Printed electrochemical strip for the detection of miRNA-29a: a possible biomarker related to Alzheimer's disease, Anal. Chem. 94 (2022) 15558–15563.
[55] J. Lim, S. Kim, S.J. Oh, S.M. Han, S.Y. Moon, B. Kang, et al., miRNA sensing hydrogels capable of self-signal amplification for early diagnosis of Alzheimer's disease, Biosens. Bioelectron. 209 (2022) 114279.
[56] B. Khalilzadeh, M. Rashidi, A. Soleimanian, H. Tajalli, G.S. Kanberoglu, B. Baradaran, et al., Development of a reliable microRNA based electrochemical genosensor for monitoring of miR-146a, as key regulatory agent of neurodegenerative disease, Int. J. Biol. Macromol. 134 (2019) 695–703.
[57] I. Arevalo-Rodriguez, N. Smailagic, M.R. i Figuls, A. Ciapponi, E. Sanchez-Perez, A. Giannakou, et al., Mini-Mental State Examination (MMSE) for the detection of

Alzheimer's disease and other dementias in people with mild cognitive impairment (MCI), Cochrane Database Syst. Rev. (2015).
[58] K.-N. Lin, H.-C. Liu, Clinical dementia rating (CDR), Chinese version, Acta Neurol. Taiwan 12 (2003) 154–165.
[59] K.C. Chen, C.Y. Weng, S. Hsiao, W.L. Tsao, M. Koo, Cognitive decline and slower reaction time in elderly individuals with mild cognitive impairment, Psychogeriatrics 17 (2017) 364–370.

Chin-Wei Lin received an M.S. from the Institute of Nanoscience at National Chung Hsing University in Taiwan in 2016. He received a Ph.D. in graduate institute of applied physics at National Taiwan University in 2022. He is now a postdoctoral researcher in Department of Physics, National Taiwan University. He is interested in nanoscience, biomedical assay, magnetic particle imaging, and superconducting materials.

Jing-Han Huang received a B.S. from the Department of Physics, National Chung Hsing University in 2022 and received an M.S. from the Institute of Nanoscience at National Chung Hsing University in Taiwan in 2024. She is interested in biomedical assay, and nanoscience.

Po-Han Lin received a Medical Doctor degree from Taipei Medical University in 2003, and a Ph.D. in clinical medicine from China Medical University (Taiwan) in 2016. He is an attending physician at the National Taiwan University Hospital and a clinical assistant professor at the Graduate Institute of Medical Genomics and Proteomics, National Taiwan University Medical School, since 2017. He now is a medical oncologist and geneticist, treating breast cancer patients, participating in clinical trials and responsible for genetic counseling and testing for patients who have the diagnosis of hereditary cancer syndrome.

Ting-Bin Chen received a degree of Doctor of Medicine from Fu Jen Catholic University in 2008 and a Ph.D. in Neuroscience from National Yang Ming University in 2020. He is now an attending neurologist in the Neurological Institute at Taichung Veterans General Hospital in Taiwan. He is interested in dementia syndromes, neuroimaging analysis, and biomarker analysis.

Li-Min Wang received the BS and MS degrees in physics from National Taiwan Normal University, Taipei, and the Ph.D. degree from National Taiwan University in 1988, 1990, and 1995, respectively. Since 2009 he has worked as a Full Professor at the Department of Physics, National Taiwan University. His research interests include the basic research of superconductivity, Josephson devices, magnetic bioassay, and transparent conductive oxide thin films.

Yu-Ching Huang is currently an Associate Professor in the Department of Materials Engineering at Ming Chi University of Technology, Taiwan. He received his PhD degree in the Institute of Materials Science and Engineering of National Taiwan University. His research interests are in printing flexible organic electronics and dim-light photovoltaics applications.

Kuen-Lin Chen received a B.S. in Physics from National Taiwan University in 1999, an M. S. in Physics from National Taiwan University in 2001, and a Ph.D. in Physics from National Taiwan University in 2008. He is now a Professor in the Institute of Nanoscience at National Chung Hsing University in Taiwan. He is interested in superconducting devices, nanoscience, magnetic bioassay, magneto-optics and magnetoplasmonics.